JEE Journal of Ecological Engineering

Journal of Ecological Engineering, 2026, 27(2), 91–101
https://doi.org/10.12911/22998993/210921
ISSN 2299–8993, License CC-BY 4.0

Received: 2025.09.02
Accepted: 2025.12.15
Published: 2026.01.15

Valorization of banana pseudostem for green synthesis of silver nanoparticle-functionalized carboxyl cellulose nanomaterial

Tu Thi Cam Tran[1,2], Vy Tuong Ngo[1,2], Hung Minh Nguyen[1,2], Tuyet-Mai Tran-Thuy[1,2], Long Quang Nguyen[1,2], Dung Van Nguyen[1,2*]

[1] Faculty of Chemical Engineering, Ho Chi Minh City University of Technology (HCMUT), 268 Ly Thuong Kiet Street, Dien Hong Ward, Ho Chi Minh City, Vietnam
[2] Vietnam National University Ho Chi Minh City, Linh Xuan Ward, Ho Chi Minh City, Vietnam
* Corresponding author;s email: nvdung@hcmut.edu.vn

ABSTRACT

Banana pseudostem (BPS), a widely available agricultural residue, is frequently underutilized and discarded following banana harvesting. Compositional analysis in this study revealed that BPS comprises 31.5 ± 0.1 wt% cellulose, 25.1 ± 0.5 wt% hemicellulose, 15.2 ± 0.0 wt% Klason lignin, 2.8 ± 0.3 wt% acid-soluble lignin, 11.5 ± 0.5 wt% dissolved organic matter, and 13.1 ± 0.2 wt% ash. The biomass was valorized into carboxyl cellulose nanomaterials (CCNMs) via a one-pot nitro-oxidation process, efficiently introducing carboxyl functional groups (up to 3.98 ± 0.02 mmol/g) onto the CCNM surface. Subsequently, silver nanoparticle-decorated CCNM (AgNPs/CCNM) was synthesized through the in situ reduction of $AgNO_3$, where CCNM served as both reducing and stabilizing agents, thereby eliminating the need for additional reagents. Characterization confirmed the formation of AgNPs (~10 nm, 2.0 wt%) anchored on the CCNM surface. Altogether, this work highlights a sustainable approach for transforming agricultural waste into high-value, functional nanomaterial for further advanced applications.

Keywords: banana pseudostem, carboxyl cellulose, nitro-oxidation, silver nanoparticle, biomass valorization, green chemistry.

INTRODUCTION

The banana plant *(Musa* spp.) is one of the most widely cultivated fruit crops worldwide, thriving in tropical and subtropical regions (Kumari et al., 2025; Maseko et al., 2024). After fruiting, the plant is harvested, leaving behind the fibrous stalk known as BPS. As a monocarpic plant, the banana produces fruit only once, and the pseudostem is cut down to allow new shoots to grow, generating substantial amounts of lignocellulosic residue (Badanayak et al., 2023; Sulaiman et al., 2023). Although still underutilized, BPS holds considerable promise as a sustainable, high-value feedstock for advanced bio-based materials and biochemical production, driving waste valorization and green chemistry in support of a circular bioeconomy (Fiallos-Cárdenas et al., 2022; Padam et al., 2014; Uljanah et al., 2024).

Growing environmental concerns over the reliance on fossil fuel–derived materials have accelerated the search for sustainable alternatives, with bio-based materials emerging as a key solution (Wu et al., 2022). Biomass valorization offers a pivotal pathway by converting low-value agricultural residues and organic wastes into high-performance products through chemical, thermal, or biological processes (Konyannik and Lavie, 2025; Ning et al., 2021). These processes enable the production of biochar, activated carbon, cellulose-based materials, lignin-derived materials, and biocomposites for diverse advanced applications (Arevalo-Gallegos et al., 2017; Nguyen et al., 2024; Tran et al., 2024). Among these, cellulose nanomaterials are particularly noteworthy due to their high surface area, superior crystallinity, excellent mechanical strength, and facile surface functionalization, making them suitable

for applications ranging from advanced packaging and barrier coatings to biomedical scaffolds and structural composites (Kassie et al., 2024; Reshmy et al., 2020).

Carboxyl cellulose nanomaterials, also referred to as oxidized cellulose nanomaterials, are obtained by introducing carboxyl (–COOH) groups onto the cellulose backbone via oxidative processes (Lam & Hemraz, 2021). Common oxidation strategies include TEMPO-mediated oxidation, periodate–chlorite oxidation, and nitro-oxidation (Duceac et al., 2022). TEMPO-mediated oxidation provides high selectivity and excellent yields but requires costly catalysts and hazardous reagents (Fernandes et al., 2023; Magagula et al., 2022). Periodate–chlorite oxidation is a multi-step, chemically intensive method. It can also cause fiber degradation under harsh conditions (Brault et al., 2025; Nypelö et al., 2021). In contrast, nitro-oxidation, which employs a nitric acid–sodium nitrite mixture, offers a more sustainable alternative (Abdel Aziz et al., 2025; Nguyen et al., 2023b). This approach integrates oxidation and partial hydrolysis in a single step, reduces chemical consumption, and supports zero-waste practices, as the effluent can be neutralized for use as fertilizer (Chen et al., 2022b; Sharma et al., 2017). Moreover, it allows direct production of CCNMs from raw biomass, making it particularly attractive for scalable and eco-friendly applications (Chen et al., 2022a; Sharma et al., 2018).

Silver nanoparticles are among the most widely studied metallic nanomaterials owing to their unique physicochemical properties, including a high surface-to-volume ratio, strong optical characteristics, remarkable catalytic activity, and potent antimicrobial efficacy (Abbas et al., 2024; Dhaka et al., 2023). These features make AgNPs highly attractive for diverse applications, including catalysis, sensing, wound healing, and antimicrobial coatings (Rodrigues et al., 2024). Conventional chemical synthesis of AgNPs typically requires toxic reducing agents (e.g., sodium borohydride, hydrazine) and stabilizers, generating hazardous by-products (Nguyen et al., 2023c; Salama et al., 2021). To overcome these drawbacks, green synthesis methods have been developed, using plant extracts, microorganisms, polysaccharides, or biopolymers as eco-friendly reducing and stabilizing agents, thereby improving sustainability and biocompatibility (Shahzadi et al., 2025; Vidyasagar et al., 2023). CCNMs, with their high density of carboxyl groups, provide negatively charged sites capable of chelating silver ions (Ag^+), facilitating uniform nucleation and strong anchoring of AgNPs (Gopiraman et al., 2015; Kaushik & Moores, 2016). This immobilization prevents particle aggregation and enhances dispersion, stability, and reusability in aqueous and catalytic systems (Lam & Hemraz, 2021; Spagnol et al., 2018). Moreover, the renewable, biodegradable, and mechanically robust nature of CCNMs aligns with green synthesis principles, enabling sustainable AgNPs/CCNM composites for various applications (Oprea & Panaitescu, 2020; Oun et al., 2020).

In this study, the chemical composition of BPS was first analyzed. Subsequently, the biomass was valorized via one-pot nitro-oxidation to produce CCNMs. The resulting material served as a support for the in situ synthesis of AgNPs from silver nitrate, eliminating the need for for external reducing and stabilizing agents.

MATERIALS AND METHODS

Banana pseudostem

BPS waste from chopped banana plants was collected from a farm in Dong Thap Province, Vietnam. The raw material was cut into small pieces, thoroughly washed with tap water, and subsequently rinsed with distilled water to remove residual impurities. The cleaned BPS was then dried in an oven at 80 °C for 24 h until completely dry. The material was ground into a fine powder and stored in an airtight container for subsequent processing. The chemical composition of BPS was analyzed using reported procedures (Nguyen et al., 2023a; Nguyen et al., 2023b). Acid-soluble lignin was measured by a Jasco V-730 UV-Vis spectrophotometer. All quantitative analyses were performed twice, and the results are presented as mean values with corresponding standard deviations. In addition, energy-dispersive X-ray (EDX) spectroscopy and elemental mapping of BPS were obtained using a JEOL JSM-IT200 system.

Synthesis of CCNM

The procedure for synthesizing CCNM from BPS was referenced in previous studies (Nguyen et al., 2023b; Nguyen and Nguyen, 2023). In a three-necked flask, 5.00 g of BPS was introduced,

followed by the addition of 75 mL of concentrated HNO_3 (65.0–68.0%). After 10 min, 10.00 g of $NaNO_2$ was added, and the mixture was stirred continuously on a hotplate stirrer at 50 °C. At the designated synthesis time, the process was stopped by adding 250 mL of distilled water to the flask, and the mixture was transferred to a 500 mL beaker. The product was rinsed with an ethanol–water mixture (1:2 v/v) and separated by centrifugation to remove waste solution. The material was allowed to settle for one day and subsequently washed daily for 4–5 days until the pH of the supernatant reached 3.5–4.0. The final product was decanted and dried at 50 °C for 2 days. Samples were denoted as CCNM-Xh, where X represents the synthesis time (h). To obtain the carboxylate ($–COO^-$) form, the suspension of CCNM was treated with aqueous $NaHCO_3$ until the pH reached ~7.5.

Synthesis of AgNPs/CCNM

0.432 g of CCNM-8h was dispersed in 100 mL of distilled water using a hotplate stirrer. $AgNO_3$ solution (2.00 mL, 0.100 M) was added dropwise, and the mixture was stirred for 3 h to enable ion exchange between Ag^+ and carboxyl groups. The suspension was then heated to 70 °C within 6 h for hydrothermal reduction of Ag^+ to AgNPs. The resulting AgNPs/CCNM was collected after filtration, thorough washing, and drying.

Characterization of CCNM and AgNPs/CCNM

X-ray diffraction (XRD) patterns of BPS, CCNM and AgNPs/CCNM samples were recorded using a Bruker D2 Phaser diffractometer. Crystallinity index (CrI) was calculated via the Segal equation (Nam et al., 2016). CCNM in the carboxylate form characterized by transmission electron microscopy (TEM) using a JEOL JEM-2100 instrument, as well as by EDX spectroscopy and elemental mapping with the aforementioned JEOL JSM-IT200 system. Fourier-transform infrared (FTIR) spectra were collected on a Bruker Tensor 27 spectrometer. Silver content in AgNPs/CCNM was quantified via ICP-OES (PerkinElmer Optima 7300 DV). Prior to analysis, silver was extracted by concentrated HNO_3. Carboxyl content was determined by ion exchange and acid–base titration: 0.100 g of CCNM was soaked in 10.0 mL of 2.00 wt% $Ca(CH_3COO)_2$ solution for 24 h, followed by titration with 0.100 M NaOH using phenolphthalein as an indicator. For each condition, two CCNM samples were synthesized and titrated in duplicate. The results were reported as mean ± standard deviation.

RESULTS AND DISCUSSION

Chemical composition of BPS

As shown in Table 1, BPS primarily comprised cellulose (31.5 ± 0.1 wt%), hemicellulose (25.1 ± 0.5 wt%), and lignin, including Klason lignin (15.2 ± 0.0 wt%) and acid-soluble lignin (2.8 ± 0.3 wt%), along with dissolved organic matter (11.5 ± 0.5 wt%) and ash (13.1 ± 0.2 wt%), yielding a total composition of 99.2 ± 1.6 wt%. These values are generally consistent with reported ranges for cellulose (31.0–54.5 wt%), total lignin (9.0–22.6 wt%), and ash (7.0–21.5 wt%) (Jayaprabha et al., 2011), although the hemicellulose content is notably higher than reported values (6.7–19.7 wt%). Such variations may arise from differences in banana cultivar, harvest maturity, the anatomical part analyzed, or analytical methods. EDX spectroscopy confirmed the dominance of C and O, along with minor amounts of Mg, K, Ca, Si, and Cl, while elemental mapping indicated a relatively uniform distribution of these elements across BPS (Figure 1). Owing to its non-woody structure and high cellulose content, BPS represents a promising feedstock for CCNM production.

Properties of CCNM

Table 2 summarizes the carboxyl content of CCNM samples synthesized at different times. The raw BPS exhibited a baseline carboxyl content of 0.55 ± 0.07 mmol/g, likely originating from the natural existence of acidic components.

Table 1. The chemical composition of BPS

Compound	Composition (wt%)	
	This research	Jayaprabha et al. (2011)
Cellulose	31.5 ± 0.1	31.0–54.5
Hemicellulose	25.1 ± 0.5	6.7–19.7
Klason lignin	15.2 ± 0.0	9.0–22.6
Acid-soluble lignin	2.8 ± 0.3	
Dissolved organic matter	11.5 ± 0.5	–
Ash	13.1 ± 0.2	7.0–21.5
Total	99.2 ± 1.6	–

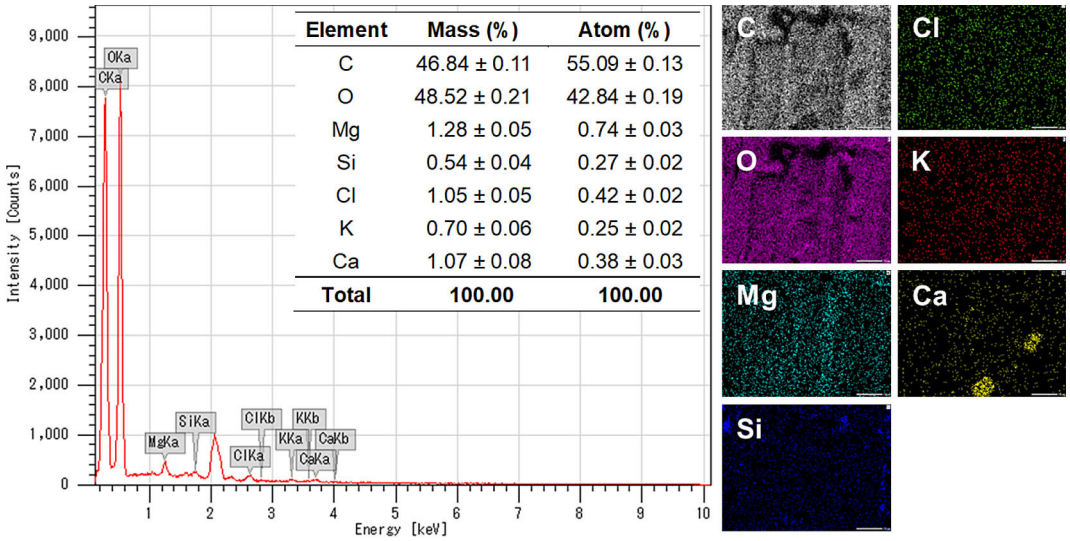

Figure 1. EDX spectroscopy and elemental mapping of BPS

Table 2. Carboxyl content of CCNM samples

Sample	Synthesis time (h)	Carboxyl content	
		(mmol/g)	(wt%)
BPS	-	0.55 ± 0.07	2.5 ± 0.3
CCNM-1h	1	2.20 ± 0.14	9.9 ± 0.6
CCNM-2h	2	3.30 ± 0.00	14.9 ± 0.0
CCNM-4h	4	3.45 ± 0.21	15.5 ± 0.9
CCNM-6h	6	3.78 ± 0.02	17.0 ± 0.1
CCNM-8h	8	3.98 ± 0.02	17.9 ± 0.1
CCNM-12h	12	3.84 ± 0.15	17.3 ± 0.7

Upon introduction of the HNO_3–$NaNO_2$ mixture, the carboxyl content increased sharply, reaching 2.20 ± 0.14 mmol/g after only 1 h. Continued synthesis further elevated the content to 3.30 ± 0.00 mmol/g at 2 h and a maximum of 3.98 ± 0.02 mmol/g (17.9 ± 0.1 wt%) at 8 h, followed by a slight decrease to 3.84 ± 0.15 mmol/g at 12 h. This trend indicates rapid oxidation of primary –CH_2OH groups into –COOH groups during the initial stages, approaching saturation as synthesis time extends, with prolonged exposure potentially causing partial decarboxylation.

Biomass mass losses during the nitro-oxidation process mainly arise from the removal of hemicellulose, lignin, and amorphous cellulose, together with partial degradation and decarboxylation under strong oxidative and acidic conditions. The BPS feedstock contained 31.5 ± 0.1 wt% cellulose, corresponding to a theoretical maximum of 1.58 g cellulose from 5.00 g BPS. In practice, side reactions during synthesis and material losses during cleaning and purification reduced the recovery. On average, ~1 g of CCNM-8h was obtained, representing a practical and sufficiently high yield for this process.

XRD patterns reveal distinct changes in crystallinity following the nitro-oxidation of BPS to CCNMs (Figure 2). Raw BPS exhibits a broad and diffuse diffraction profile with a low CrI of 31%, indicating a largely amorphous structure. Upon one-pot nitro-oxidation, sharper peaks emerge at $2\theta \approx 15.6°$ and 22.7°, corresponding to the (110) and (200) planes of cellulose, demonstrating the preservation of native crystalline regions. CrI increases markedly to 75% for CCNM-4h and further to 76% for CCNM-8h and CCNM-12h, indicating that prolonged reaction did not significantly alter the crystalline fraction beyond initial enhancement. This substantial rise in CrI suggests that nitro-oxidation preferentially removed amorphous hemicellulose and lignin, exposing highly ordered cellulose domains. The retention of cellulose structure alongside enhanced crystallinity underscores the suitability of CCNMs for applications requiring high structural order and functional surface chemistry.

The FTIR spectra (Figure 3) reveal the chemical transformations of BPS during its conversion to CCNMs. Raw BPS displays characteristic lignocellulosic features, including a broad O–H stretching band around 3420 cm^{-1}, C–H stretching near 2925 cm^{-1}, and a strong peak at 1635 cm^{-1} attributed to C=O stretching of hemicellulose acetyl groups and aromatic skeletal vibrations of lignin. After nitro-oxidation, a distinct

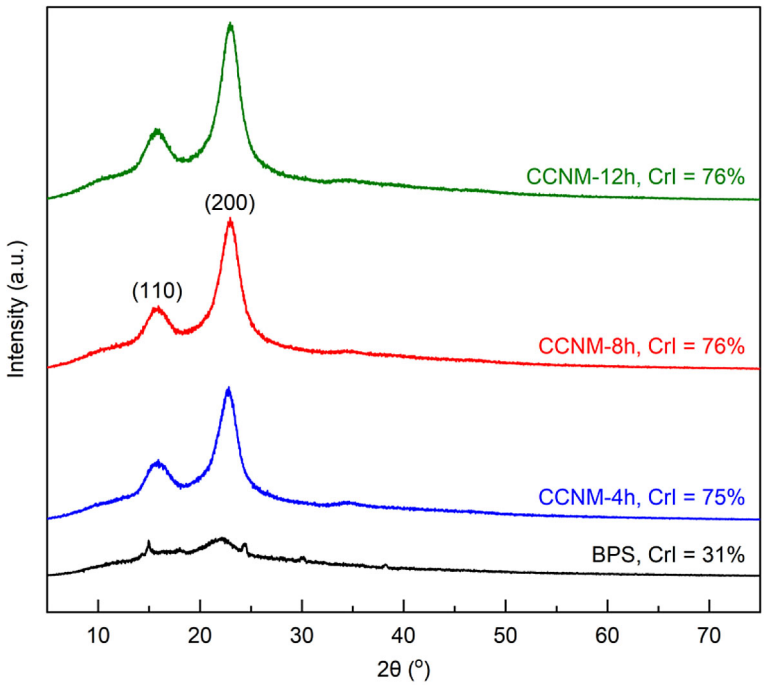

Figure 2. XRD patterns of BPS and CCNM samples

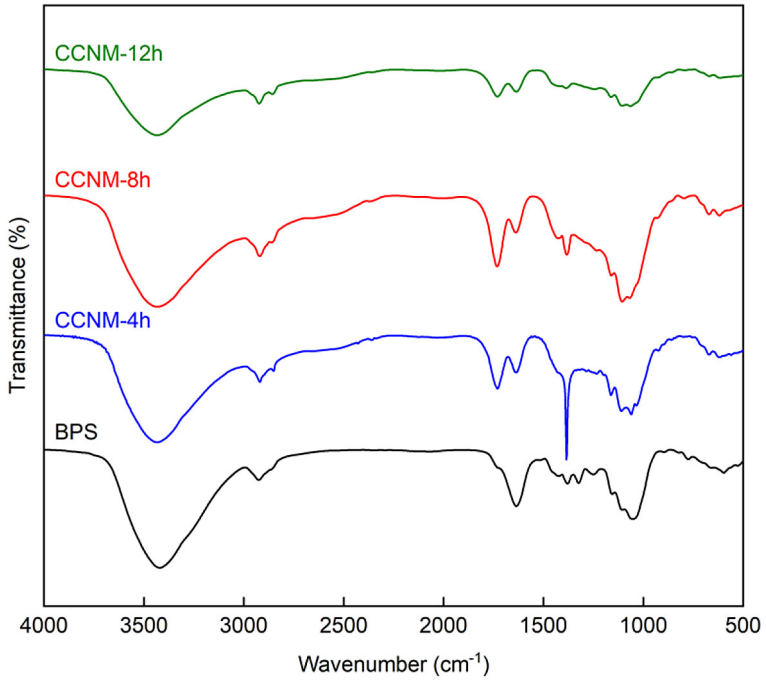

Figure 3. FTIR spectra of BPS and CCNM samples

absorption band at 1730 cm^{-1}, corresponding to the C=O stretching of carboxyl groups, appears and intensifies with synthesis time up to 8 h, indicating progressive surface oxidation. Peaks at 1030–1050 cm^{-1}, characteristic of C–O–C stretching in cellulose, remained visible, confirming preservation of the polysaccharide backbone. However, a general decrease in peak intensity from 8 to 12 h suggests partial loss or alteration of certain functional groups under prolonged reaction. These spectral changes confirm the successful introduction of carboxyl functionalities and the selective removal of non-cellulosic components, consistent with carboxyl

content and XRD results. Figure 4 reveals that the CCNM-8h sample exhibits nanoscale morphologies composed of nearly spherical to slightly irregular particles, with sizes estimated at approximately 10–40 nm. These nanoparticles exhibit a prominent tendency to form loosely clustered aggregates. This agglomeration likely stems from robust hydrogen bonding among abundant surface –COOH groups and adjacent –OH moieties, which not only facilitate interparticle adhesion but also promote minimization of surface energy, favoring a rounded, spherical morphology. This behavior aligns with the self-assembly tendencies of cellulose nanomaterials driven by non-covalent forces such as hydrogen bonding, van der Waals interactions, and electrostatics (Carvalho et al., 2021; Doan and Chiang, 2022; Sanchez-Salvador et al., 2023).

Compared with BPS, CCNM-8h retained C and O (Figure 5). Introduction of $NaHCO_3$ to the CCNM-8h sample resulted in a high Na content (13.54 ± 0.11 wt%), corresponding to Na^+ ions counterbalancing the negatively charged carboxylate groups. Collectively, evidence from acid–base titration, FTIR spectroscopy, and EDX analysis confirms the successful incorporation of carboxyl functionalities into the CCNM structure.

Properties of AgNPs/CCNM

The XRD pattern of AgNPs/CCNM exhibits characteristic diffraction peaks of cellulose and metallic silver, confirming the successful hybrid

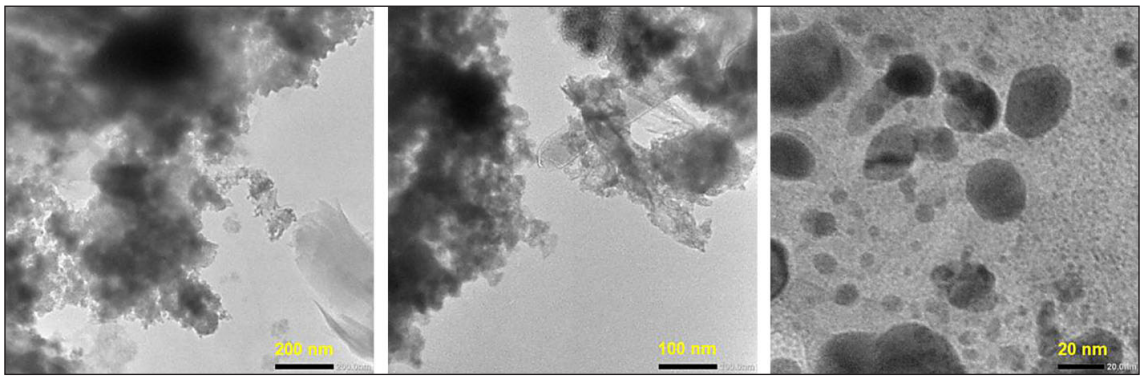

Figure 4. TEM images of CCNM-8h

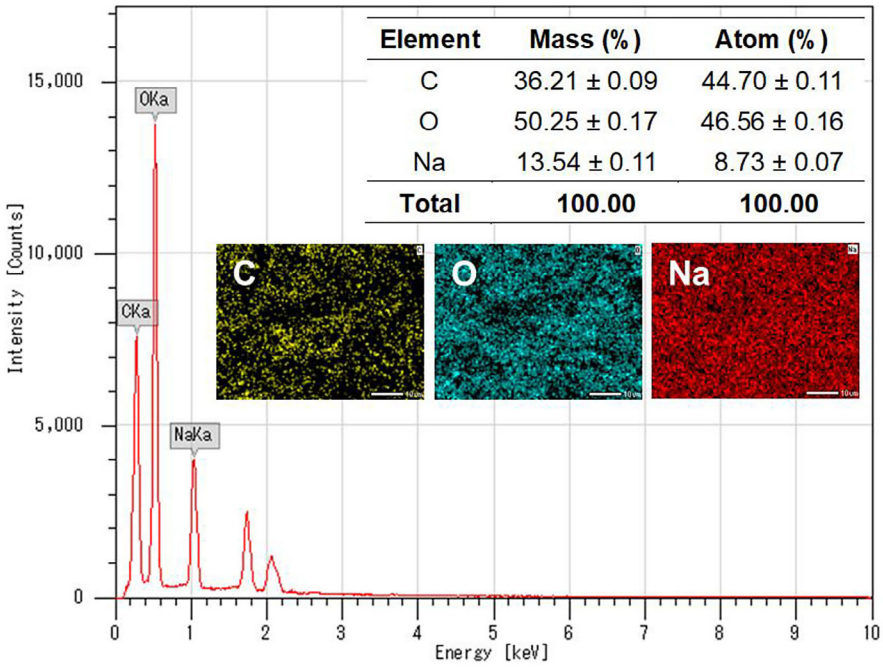

Figure 5. EDX spectroscopy and elemental mapping of CCNM-8h

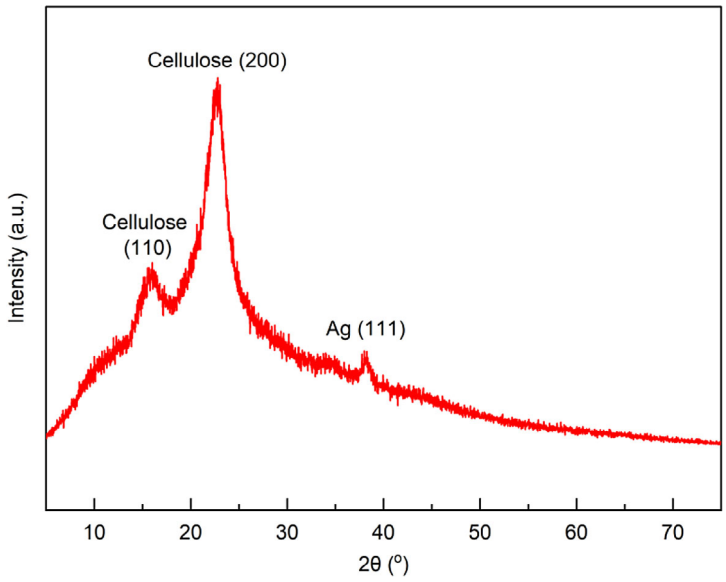

Figure 6. XRD pattern of AgNPs/CCNM

formation (Figure 6). Similar to pristine CCNM-8h, prominent peaks at 2θ = 15.6° and 22.7° for cellulose crystals remained after silver loading. A weak but discernible peak at 2θ = 38.2° is indexed to the (111) plane of face-centered cubic silver, verifying the presence of AgNPs on the CCNM surface. ICP-OES analysis further confirmed a silver content of 2.0 wt% present in AgNPs/CCNM. These findings demonstrate that AgNPs were successfully anchored to the CCNM support.

Figure 7 presents TEM micrographs of AgNPs/CCNM, revealing the successful decoration of CCNM with AgNPs. At a relatively low silver content (2.0 wt%), AgNPs appear as distinct, high-contrast dots due to their strong electron-scattering ability, with an estimated particle size of approximately 10 nm. The lighter matrix corresponds to clustered spherical CCNM domains, which preserve their nanoscale morphology after silver incorporation. Mild agglomeration is evident, likely driven by hydrogen bonding among surface –COOH and –OH groups of CCNM, which provide nucleation sites for anchoring AgNPs.

As depicted in Figure 8, EDX spectroscopy of AgNPs/CCNM confirms the successful incorporation of silver, showing a high surface content of 9.51 ± 0.20 wt%. This value is significantly higher than the bulk silver content (2.0 wt%) obtained from ICP-OES, indicating that AgNPs are predominantly anchored on the CCNM surface rather than embedded within the matrix. Elemental mapping further demonstrates the homogeneous distribution of silver alongside carbon and oxygen, evidencing uniform surface decoration at the microscale. As shown in Figure 9, CCNM-8h and AgNPs/CCNM exhibit similar FTIR spectra, indicating that the structure of CCNM remains largely after AgNP decoration. However, subtle spectral changes are evident, including a reduced intensity of the O–H band and minor shifts in the C=O region for AgNPs/CCNM. These variations suggest weak interactions between AgNPs and

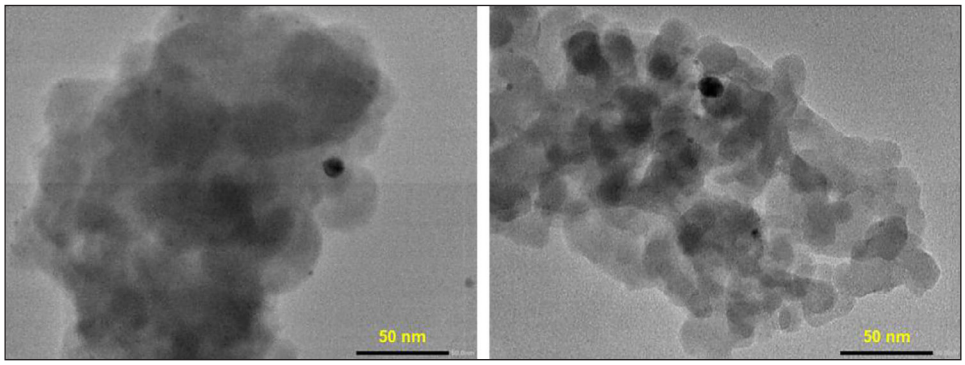

Figure 7. TEM images of AgNPs/CCNM

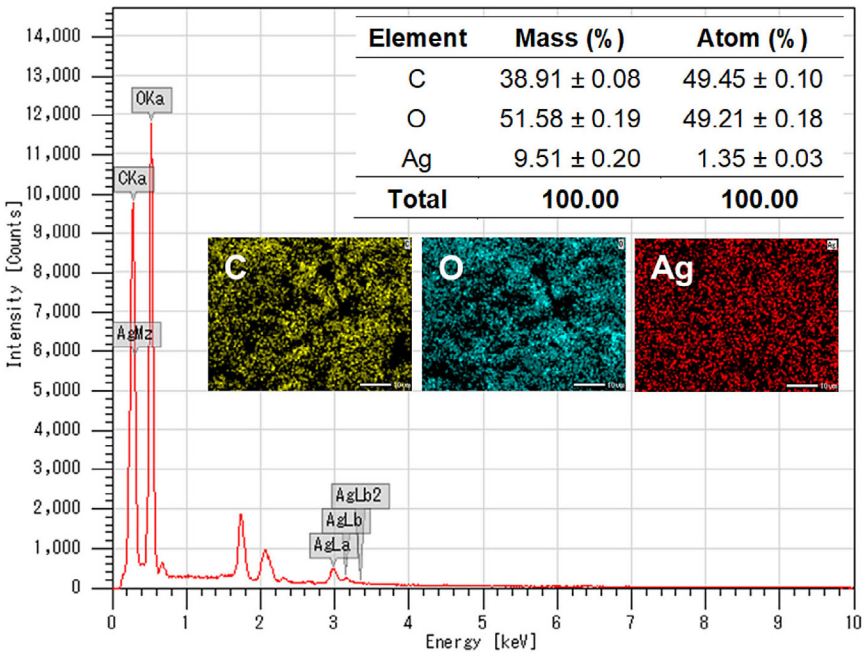

Figure 8. EDX spectroscopy and elemental mapping of AgNPs/CCNM

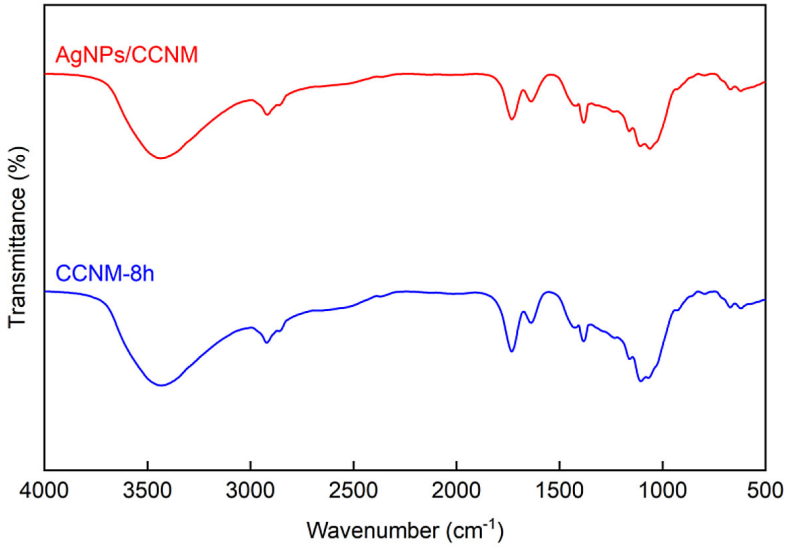

Figure 9. FTIR spectra of CCNM-8h and AgNPs/CCNM

oxygen-containing functional groups, which enable nanoparticle anchoring without disrupting the underlying matrix (Sambalova et al., 2018; Uznanski and Bryszewska, 2010).

CONCLUSIONS

This study demonstrates a green valorization pathway for banana pseudostem, which contains 31.5 ± 0.1 wt% cellulose, 25.1 ± 0.5 wt% hemicellulose, 15.2 ± 0.0 wt% Klason lignin, 2.8 ± 0.3 wt% acid-soluble lignin, 11.5 ± 0.5 wt% dissolved organic matter, and 13.1 ± 0.2 wt% ash, into high-value nanomaterials. Through a one-pot nitro-oxidation process, BPS was converted to carboxyl cellulose nanomaterials with a maximum carboxyl content of 3.98 ± 0.02 mmol/g (17.9 ± 0.1 wt%) and the crystallinity index rising from 31% (BPS) to 76% (CCNM-8h). TEM analysis revealed nanoscale spherical particles of ~10–40 nm, while FTIR confirmed the emergence of a C=O

stretching band at 1730 cm^{-1}, indicative of carboxyl group formation. Subsequent in situ synthesis produced AgNPs/CCNM containing ~2.0 wt% silver (ICP-OES), with a particle size of ~10 nm. These findings confirm the successful production of structurally ordered, surface-functionalized nanomaterials using only biomass and benign reagents. The AgNPs/CCNM hybrid offers potential for applications in catalysis, antimicrobial systems, and environmental remediation, underscoring the role of agricultural residues as sustainable feedstocks for advanced nanomaterial fabrication.

Acknowledgments

We acknowledge Ho Chi Minh City University of Technology (HCMUT), VNU-HCM for supporting this study.

REFERENCES

1. Abbas, R., Luo, J., Qi, X., Naz, A., Khan, I. A., Liu, H., Yu, S., Wei, J. (2024). Silver nanoparticles: Synthesis, structure, properties and applications. *Nanomaterials*, *14*(17), 1425. https://doi.org/10.3390/nano14171425
2. Abdel Aziz, Y. S., Liu, A., Yu, S., Hsiao, B. S. (2025). Nitro-oxidation process for sustainable production of carboxylated lignin-containing cellulose nanofibers from sugarcane bagasse. *Carbohydrate Polymers*, *368*, 124109. https://doi.org/10.1016/j.carbpol.2025.124109
3. Arevalo-Gallegos, A., Ahmad, Z., Asgher, M., Parra-Saldivar, R., Iqbal, H. M. N. (2017). Lignocellulose: A sustainable material to produce value-added products with a zero waste approach—A review. *International Journal of Biological Macromolecules*, *99*, 308-318. https://doi.org/10.1016/j.ijbiomac.2017.02.097
4. Badanayak, P., Jose, S., Bose, G. (2023). Banana pseudostem fiber: A critical review on fiber extraction, characterization, and surface modification. *Journal of Natural Fibers*, *20*(1), 2168821. https://doi.org/10.1080/15440478.2023.2168821
5. Brault, L., Marlin, N., Mortha, G., Boucher, J., Lachenal, D. (2025). Periodate-chlorite oxidation for dicarboxylcellulose (DCC) production: activation strategies for the dissolution and visualization of oxidized groups distribution. *Cellulose*, *32*(2), 723-742. https://doi.org/10.1007/s10570-024-06312-x
6. Carvalho, J. P. F., Silva, A. C. Q., Silvestre, A. J. D., Freire, C. S. R., Vilela, C. (2021). Spherical cellulose micro and nanoparticles: A review of recent developments and applications. *Nanomaterials*, *11*(10), 2744. https://doi.org/10.3390/nano11102744
7. Chen, H., Chi, K., Cao, R., Sharma, S. K., Bokhari, S. M. Q., Johnson, K. I., Li, D., Sharma, P. R., Hsiao, B. S. (2022a). Nitro-oxidation process for fabrication of efficient bioadsorbent from lignocellulosic biomass by combined liquid-gas phase treatment. *Carbohydrate Polymer Technologies and Applications*, *3*, 100219. https://doi.org/10.1016/j.carpta.2022.100219
8. Chen, H., Sharma, P. R., Sharma, S. K., Alhamzani, A. G., Hsiao, B. S. (2022b). Effective thallium(i) removal by nanocellulose bioadsorbent prepared by nitro-oxidation of sorghum stalks. *Nanomaterials*, *12*(23), 4156. https://doi.org/10.3390/nano12234156
9. Dhaka, A., Chand Mali, S., Sharma, S., Trivedi, R. (2023). A review on biological synthesis of silver nanoparticles and their potential applications. *Results in Chemistry*, *6*, 101108. https://doi.org/10.1016/j.rechem.2023.101108
10. Doan, T. K. Q., Chiang, K. Y. (2022). Characteristics and kinetics study of spherical cellulose nanocrystal extracted from cotton cloth waste by acid hydrolysis. *Sustainable Environment Research*, *32*(1), 26. https://doi.org/10.1186/s42834-022-00136-9
11. Duceac, I. A., Tanasa, F., Coseri, S. (2022). Selective oxidation of cellulose—A multitask platform with significant environmental impact. *Materials*, *15*(14), 5076. https://doi.org/10.3390/ma15145076
12. Fernandes, A., Cruz-Lopes, L., Esteves, B., Evtuguin, D. (2023). Nanotechnology applied to cellulosic materials. *Materials*, *16*(8), 3104. https://doi.org/10.3390/ma16083104
13. Fiallos-Cárdenas, M., Pérez-Martínez, S., Ramirez, A. D. (2022). Prospectives for the development of a circular bioeconomy around the banana value chain. *Sustainable Production and Consumption*, *30*, 541-555. https://doi.org/10.1016/j.spc.2021.12.014
14. Gopiraman, M., Bang, H., Yuan, G., Yin, C., Song, K.-H., Lee, J. S., Chung, I. M., Karvembu, R., Kim, I. S. (2015). Noble metal/functionalized cellulose nanofiber composites for catalytic applications. *Carbohydrate Polymers*, *132*, 554-564. https://doi.org/10.1016/j.carbpol.2015.06.051
15. Jayaprabha, J. S., Brahmakumar, M., Manilal, V. B. (2011). Banana pseudostem characterization and its fiber property evaluation on physical and bioextraction. *Journal of Natural Fibers*, *8*(3), 149-160. https://doi.org/10.1080/15440478.2011.601614
16. Kassie, B. B., Daget, T. M., Tassew, D. F. (2024). Synthesis, functionalization, and commercial application of cellulose-based nanomaterials. *International Journal of Biological Macromolecules*, *278*, 134990. https://doi.org/10.1016/j.ijbiomac.2024.134990

17. Kaushik, M., Moores, A. (2016). Review: nanocelluloses as versatile supports for metal nanoparticles and their applications in catalysis. *Green Chemistry*, *18*(3), 622-637. https://doi.org/10.1039/C5GC02500A
18. Konyannik, B. Y., Lavie, J. D. (2025). Valorization techniques for biomass waste in energy Generation: A systematic review. *Bioresource Technology*, *435*, 132973. https://doi.org/10.1016/j.biortech.2025.132973
19. Kumari, S., Debbarma, R., Habibi, M., Haque, S., Suprasanna, P. (2025). Banana waste valorisation and the development of biodegradable biofilms. *Waste Management Bulletin*, *3*(3), 100213. https://doi.org/10.1016/j.wmb.2025.100213
20. Lam, E., Hemraz, U. D. (2021). Preparation and surface functionalization of carboxylated cellulose nanocrystals. *Nanomaterials*, *11*(7), 1641. https://doi.org/10.3390/nano11071641
21. Magagula, L. P., Masemola, C. M., Ballim, M. A. a., Tetana, Z. N., Moloto, N., Linganiso, E. C. (2022). Lignocellulosic biomass waste-derived cellulose nanocrystals and carbon nanomaterials: A review. *International Journal of Molecular Sciences*, *23*(8), 4310. https://doi.org/10.3390/ijms23084310
22. Maseko, K. H., Regnier, T., Meiring, B., Wokadala, O. C., Anyasi, T. A. (2024). *Musa* species variation, production, and the application of its processed flour: A review. *Scientia Horticulturae*, *325*, 112688. https://doi.org/10.1016/j.scienta.2023.112688
23. Nam, S., French, A. D., Condon, B. D., Concha, M. (2016). Segal crystallinity index revisited by the simulation of X-ray diffraction patterns of cotton cellulose Iβ and cellulose II. *Carbohydrate Polymers*, *135*, 1–9. https://doi.org/10.1016/j.carbpol.2015.08.035
24. Nguyen, D. V., Duong, C. T. T., Vu, C. N. M., Nguyen, H. M., Pham, T. T., Tran-Thuy, T.-M., Nguyen, L. Q. (2023a). Data on chemical composition of coffee husks and lignin microparticles as their extracted product. *Data in Brief*, *51*, 109781. https://doi.org/10.1016/j.dib.2023.109781
25. Nguyen, D. V., Ho, V. Q., Dinh, T. V., Ngo, V. T., Tran, T. T. C., Nguyen, H. M., Pham, T. T., Tran-Thuy, T.-M., Nguyen, L. Q. (2023b). Chemical composition of underutilized nipa (*Nypa fruticans*) frond and its valorization for one-pot fabrication of carboxyl cellulose nanocrystals. *Chemical Data Collections*, *46*, 101051. https://doi.org/10.1016/j.cdc.2023.101051
26. Nguyen, D. V., Nguyen, D. T., Tran, V. L. T., Vo, K. D., Nguyen, L. Q. (2023c). Preparation, characterization, and antibacterial activity of silver nanoparticle-decorated ordered mesoporous carbon. *Engineering, Technology & Applied Science Research*, *13*(3), 10828–10833. https://doi.org/10.48084/etasr.5782
27. Nguyen, D. V., Nguyen, H. T. N. (2023). High carboxyl content cellulose nanofibers from banana peel via one-pot nitro-oxidative fabrication. *Revue des Composites et des Materiaux Avances*, *33*(2), 127–133. https://doi.org/10.18280/rcma.330208
28. Nguyen, N. T. K., Le, D. T. T., Vo, K. D., Huynh, L. T., Nguyen, H. M., Tran-Thuy, T.-M., Nguyen, L. Q., Nguyen, D. V. (2024). Valorization of tropical almond (*Terminalia catappa*) leaves into iron-containing activated carbon for rapid catalytic degradation of methylene blue with hydrogen peroxide. *Journal of Ecological Engineering*, *25*(8), 54–61. https://doi.org/10.12911/22998993/189672
29. Ning, P., Yang, G., Hu, L., Sun, J., Shi, L., Zhou, Y., Wang, Z., Yang, J. (2021). Recent advances in the valorization of plant biomass. *Biotechnology for Biofuels*, *14*(1), 102. https://doi.org/10.1186/s13068-021-01949-3
30. Nypelö, T., Berke, B., Spirk, S., Sirviö, J. A. (2021). Review: Periodate oxidation of wood polysaccharides—Modulation of hierarchies. *Carbohydrate Polymers*, *252*, 117105. https://doi.org/10.1016/j.carbpol.2020.117105
31. Oprea, M., Panaitescu, D. M. (2020). Nanocellulose hybrids with metal oxides nanoparticles for biomedical applications. *Molecules*, *25*(18), 4045. https://doi.org/10.3390/molecules25184045
32. Oun, A. A., Shankar, S., Rhim, J.-W. (2020). Multifunctional nanocellulose/metal and metal oxide nanoparticle hybrid nanomaterials. *Critical Reviews in Food Science and Nutrition*, *60*(3), 435–460. https://doi.org/10.1080/10408398.2018.1536966
33. Padam, B. S., Tin, H. S., Chye, F. Y., Abdullah, M. I. (2014). Banana by-products: an under-utilized renewable food biomass with great potential. *Journal of Food Science and Technology*, *51*(12), 3527–3545. https://doi.org/10.1007/s13197-012-0861-2
34. Reshmy, R., Philip, E., Paul, S. A., Madhavan, A., Sindhu, R., Binod, P., Pandey, A., Sirohi, R. (2020). Nanocellulose-based products for sustainable applications-recent trends and possibilities. *Reviews in Environmental Science and Bio/Technology*, *19*(4), 779–806. https://doi.org/10.1007/s11157-020-09551-z
35. Rodrigues, A. S., Batista, J. G. S., Rodrigues, M. Á. V., Thipe, V. C., Minarini, L. A. R., Lopes, P. S., Lugão, A. B. (2024). Advances in silver nanoparticles: a comprehensive review on their potential as antimicrobial agents and their mechanisms of action elucidated by proteomics. *Frontiers in Microbiology*, *15*, 1440065. https://doi.org/10.3389/fmicb.2024.1440065
36. Salama, A., Abouzeid, R. E., Owda, M. E., Cruz-Maya, I., Guarino, V. (2021). Cellulose–silver composites materials: preparation and applications. *Biomolecules*, *11*(11), 1684. https://doi.org/10.3390/biom11111684

37. Sambalova, O., Thorwarth, K., Heeb, N. V., Bleiner, D., Zhang, Y., Borgschulte, A., Kroll, A. (2018). Carboxylate functional groups mediate interaction with silver nanoparticles in biofilm matrix. *ACS Omega*, *3*(1), 724–733. https://doi.org/10.1021/acsomega.7b00982

38. Sanchez-Salvador, J. L., Xu, H., Balea, A., Negro, C., Blanco, A. (2023). Nanocellulose from a colloidal material perspective. *Frontiers in Materials*, *10*, 1231404. https://doi.org/10.3389/fmats.2023.1231404

39. Shahzadi, S., Fatima, S., ul ain, Q., Shafiq, Z., Janjua, M. R. S. A. (2025). A review on green synthesis of silver nanoparticles (SNPs) using plant extracts: a multifaceted approach in photocatalysis, environmental remediation, and biomedicine. *RSC Advances*, *15*(5), 3858–3903. https://doi.org/10.1039/D4RA07519F

40. Sharma, P. R., Joshi, R., Sharma, S. K., Hsiao, B. S. (2017). A simple approach to prepare carboxycellulose nanofibers from untreated biomass. *Biomacromolecules*, *18*(8), 2333–2342. https://doi.org/10.1021/acs.biomac.7b00544

41. Sharma, P. R., Zheng, B., Sharma, S. K., Zhan, C., Wang, R., Bhatia, S. R., Hsiao, B. S. (2018). High aspect ratio carboxycellulose nanofibers prepared by nitro-oxidation method and their nanopaper properties. *ACS Applied Nano Materials*, *1*(8), 3969–3980. https://doi.org/10.1021/acsanm.8b00744

42. Spagnol, C., Fragal, E. H., Pereira, A. G. B., Nakamura, C. V., Muniz, E. C., Follmann, H. D. M., Silva, R., Rubira, A. F. (2018). Cellulose nanowhiskers decorated with silver nanoparticles as an additive to antibacterial polymers membranes fabricated by electrospinning. *Journal of Colloid and Interface Science*, *531*, 705–715. https://doi.org/10.1016/j.jcis.2018.07.096

43. Sulaiman, S. M., Nugroho, G., Saputra, H. M., Djaenudin, D., Permana, D., Fitria, N., Putra, H. E. (2023). Valorization of banana bunch waste as a feedstock via hydrothermal carbonization for energy purposes. *Journal of Ecological Engineering*, *24*(7), 61–74. https://doi.org/10.12911/22998993/163350

44. Tran, T. T. C., Phan, A. T. N., Nguyen, H. M., Nguyen, L. Q., Tran-Thuy, T.-M., Le, T. X., Nguyen, D. V. (2024). Simple fabrication of copper nanoparticle-loaded biochar from rosemary extraction residues for peroxydisulfate activation towards Ponceau 4R decolorization. *Journal of Ecological Engineering*, *25*(10), 136–145. https://doi.org/10.12911/22998993/191950

45. Uljanah, D., Melwita, E., Novia, N. (2024). Bioethanol fermentation from banana pseudostems waste (*Musa balbisiana*) pretreated with potassium hydroxide microwave. *Journal of Ecological Engineering*, *25*(9), 1–13. https://doi.org/10.12911/22998993/190691

46. Uznanski, P., Bryszewska, E. (2010). Synthesis of silver nanoparticles from carboxylate precursors under hydrogen pressure. *Journal of Materials Science*, *45*(6), 1547–1552. https://doi.org/10.1007/s10853-009-4122-3

47. Vidyasagar, Patel, R. R., Singh, S. K., Singh, M. (2023). Green synthesis of silver nanoparticles: methods, biological applications, delivery and toxicity. *Materials Advances*, *4*(8), 1831–1849. https://doi.org/10.1039/D2MA01105K

48. Wu, S., Shi, W., Li, K., Cai, J., Chen, L. (2022). Recent advances on sustainable bio-based materials for water treatment: Fabrication, modification and application. *Journal of Environmental Chemical Engineering*, *10*(6), 108921. https://doi.org/10.1016/j.jece.2022.108921